J Solid State Electrochem (2010) 14:1205–1211
DOI 10.1007/s10008-009-0955-6

ORIGINAL PAPER

RuO_2/Co_3O_4 thin films prepared by spray pyrolysis technique for supercapacitors

Yanhua Li · Kelong Huang · Dongming Zeng · Suqin Liu · Zufu Yao

Received: 21 June 2009 / Revised: 26 September 2009 / Accepted: 8 October 2009 / Published online: 5 November 2009

Abstract RuO_2/Co_3O_4 thin films with different RuO_2 content were successfully prepared on fluorine-doped tin oxide coated glass plate substrates by spray pyrolysis method, and their capacitive behavior was investigated. Electrochemical property was performed by cyclic voltammetry, constant current charge/discharge, and electrochemical impedance spectra. The capacitive performance of RuO_2/Co_3O_4 thin films with different RuO_2 content corresponded to a contribution from a main pseudocapacitance and an additional electric double-layer capacitance. The specific capacitance of pure Co_3O_4, 15.5%, 35.6%, and 62.3% RuO_2 composites at the current density of 0.2 A g^{-1} were 394±8, 453±9, 520±10, and 690±14 F g^{-1}, respectively; 62.3% RuO_2 composite presented the highest specific capacitance value at various current densities, whereas 35.6% RuO_2 composite exhibited not only the largest specific capacitance contribution from RuO_2 (C_{sp}^{RuO2}) at the current density of 0.5, 1.0, 1.5, and 2.0 A g^{-1} but also the highest specific capacitance retention ratio (46.3±2.8%) at the current density ranging from 0.2 to 2.0 A g^{-1}. Electrochemical impedance spectra showed that the contact resistance dropped gradually with the decrease of RuO_2 content, and the charge-transfer resistance (R_{ct}) increased gradually with the decrease of RuO_2 content.

Y. Li · K. Huang (✉) · D. Zeng · S. Liu · Z. Yao
College of Chemistry and Chemical Engineering,
Central South University,
Changsha, Hunan 410083, People's Republic of China
e-mail: klhuang@mail.csu.edu.cn

Y. Li
Department of Chemical Engineering and Environmental Protection,
Changsha Aeronautical Vocational and Technical College,
Changsha, Hunan 410124, People's Republic of China

Keywords Supercapacitors · RuO_2/Co_3O_4 composites · Spray pyrolysis · Electrochemical properties

Introduction

There is currently a great deal of interest in electrochemical capacitors due to their increasing demand for energy storage devices such as high power delivery devices for hybrid electric vehicles, digital telecommunication systems, backup-power storage for computers, and pulse laser technique. To date, activated carbons [1, 2], amorphous hydrous ruthenium oxide ($RuO_2{\cdot}xH_2O$) [3–6], manganese oxide [7–10], nickel oxide [11–13], cobalt oxide [14–17], $Co(OH)_2$ [18], $Ni(OH)_2$ [19], and conducting polymers [20, 21] have been extensively used as electrode materials for electrochemical capacitors. Among the metal oxides, the noble metal oxides such as amorphous ruthenium oxide have been found to possess high energy storage capabilities with large specific capacitance and good reversibility. However, the lack of abundance and high cost of the noble metal oxides inhibit commercial applications. Therefore, efforts have been made to find inexpensive alternative materials (such as manganese oxide [7–9], nickel oxide [11–13], cobalt oxide [14–17] and tin oxide [22]) or loading of RuO_2 in other cheap materials (such as RuO_2/NiO [23, 24], RuO_2/SnO_2 [25], RuO_2/TiO_2 [26], RuO_2/carbon nanotube [27], and RuO_2/mesoporous carbon [28]). All above studies have shown that loading of RuO_2 in other transition metal oxides have good capacitive behavior due to incorporation of other transition metal oxides into RuO_2 structure [29].

Co_3O_4 materials are widely used in many fields such as catalyst, solar cells, the microelectronics, and lithium-ion batteries. Even if the cycle reversibility is not good, Co_3O_4 has been suggested as a promising electrode material for supercapacitors because of its favorable pseudocapacitive performance, low cost, long-term performance, and good corrosion stability [14–16]. Thus far, some papers have been reported about Co_3O_4 or Co_3O_4/other metal oxides for supercapacitor electrode materials. For example, Chuan et al. fabricated cobalt oxide by the sol–gel process [16]. The largest specific capacitance of cobalt oxide single electrode was 291 F g^{-1}. Shinde et al. constructed Co_3O_4 thin films by spray pyrolysis. The specific capacitance of spray deposited Co_3O_4 film electrode was 74 F g^{-1} [15]. RuO_2/Co_3O_4 electrodes prepared by thermal decomposition method and one-step coprecipitation method were studied in alkaline solutions which showed good electrochemical behavior [29, 30].

Spray pyrolysis is a promising technique for fabrication of metal oxide films or metal oxide composites films. In comparison to other means, spray pyrolysis deposition of metal oxides used as electrodes in electrochemical supercapacitors has the following apparent features: (1) spray pyrolysis is a simple and economic available method [31] and (2) the prepared procedure involves none of the acetylene black and polytetrafluoroethylene. However, there are very few reports on metal oxides prepared by spray pyrolysis technique for supercapacitors [15, 31].

Based on all the above viewpoints, RuO_2/Co_3O_4 thin films with various ratios are expected to be promising electrode materials for electrochemical supercapacitors. In the present work, RuO_2/Co_3O_4 thin films were fabricated on fluorine-doped tin oxide (FTO) coated glass plate substrates by spray pyrolysis method, and their capacitive behavior was investigated. High-rate charge–discharge and the specific capacitance contribution from RuO_2 were the important factors of RuO_2/Co_3O_4 thin films used as supercapacitor electrode materials. Therefore, the specific capacitance retention ratio and the specific capacitance contribution from RuO_2 in RuO_2/Co_3O_4 thin films were studied. To the best of our knowledge, there are no reports on supercapacitive characterization of RuO_2/Co_3O_4 thin films prepared by spray pyrolysis method.

Experimental

All reagents used in this experiment were of analytical grade without further purification. All of the solutions were prepared with water purified by a Millipore Milli-Q Plus 185 purification system. A FTO coated glass plate (R=40 Ω cm^{-2}) was used as the substrate. Prior to be deposited, the substrate was ultrasonically cleaned in acetone and then alcohol and finally washed with deionized water.

RuO_2/Co_3O_4 thin films were deposited on FTO substrates by spray pyrolysis technique by spraying a mixed solution of $RuCl_3$ and $Co(CH_3COO)_2{\cdot}4H_2O$. The total concentration of $RuCl_3$ and $Co(CH_3COO)_2{\cdot}4H_2O$ solution was 0.02 M; the molar ratios of $RuCl_3/Co(CH_3COO)_2{\cdot}4H_2O$ were 1:0, 9:1, 3:1, and 1:1, respectively. The spray rate was about 2 $cm^3 min^{-1}$ through the nozzle, and the spray time was 30 min. Compressed air was used as a carrier gas. The temperature of spray pyrolysis technique was 400 °C. Further details on spray pyrolysis technique can be found in [15]. The corresponding weight percents of $RuO_2/(RuO_2 + Co_3O_4)$ were 0%, 15.5%, 35.6%, and 62.3%, respectively. The weight of RuO_2/Co_3O_4 thin films was determined using a sensitive electronic analytical balance with 0.1 mg nominal sensitivity. The specific weight of RuO_2/Co_3O_4 thin films was about 8.5 mg cm^{-2}. The experimental error to determine the composite weight was within ±2%.

X-ray diffraction (XRD) pattern was recorded on a D8 Advance Bruker X-ray diffractometer with monochromatized CuK_α (λ=1.5406 Å) incident radiation, scan range from 10° to 70° (2θ). The operation voltage was 40 kV and the current was 250 mA. The morphology of Co_3O_4/RuO_2 thin films was observed by scanning electron microscopy (FEI, Sirion200). Electrochemical studies of the as-obtained electrodes were evaluated by cyclic voltammetry (CV), constant current charge/discharge, and electrochemical impedance spectra using a CHI 660B electrochemical workstation (Shanghai, China) in a conventional three-electrode cell. The working electrodes with the geometric surface area of 1 cm^2 were the as-prepared RuO_2/Co_3O_4 thin films. A Pt plate and a saturated calomel electrode (SCE) were used as the counter and reference electrodes, respectively. A SCE was immersed into saturation solution of KCl. A 2-M KOH solution was used as the electrolyte. All the electrochemical measurements were carried out at room temperature. Cyclic voltammetry was performed at a potential range from −0.4 to 0.46 V, and constant current charge/discharge was conducted with different current densities from 0.2 to 2.0 A g^{-1} at a potential range from 0 to 0.4 V. The impedance spectra were recorded by applying an alternating current voltage of 5-mV amplitude in the frequency range from 0.01 Hz to 100 KHz.

Results and discussion

XRD analyses

Figure 1 displays XRD patterns of pure Co_3O_4 (a) and 62.3% RuO_2 composite (b). The peaks in curve (a) are assigned to Co_3O_4 (JCPDS No. 73-1701) and FTO substrate (JCPDS No. 46-1088). The crystallite size is estimated from Scherrer formula (Eq. 1)

$$D = \frac{0.9\lambda}{\beta\cos\theta} \quad (1)$$

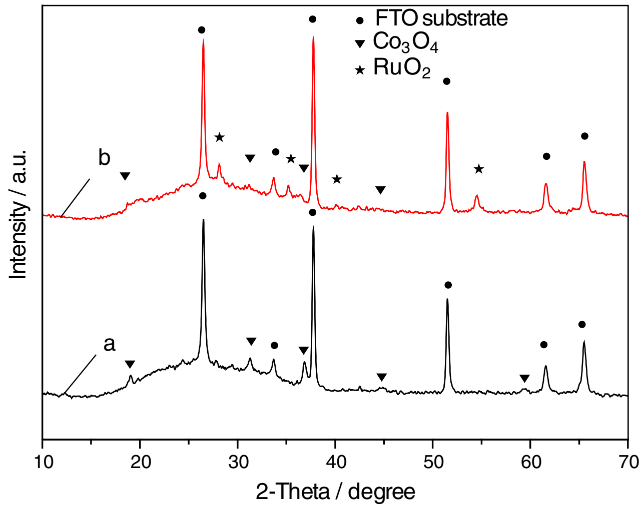

Fig. 1 XRD patterns of pure Co_3O_4 (*a*) and 62.3% RuO_2 composite (*b*)

where D is the crystallite size, λ is the X-ray radiation wavelength (λ=1.5406 Å), β is the peak width at half-maximum height of the broadening of diffraction line, and θ is the corresponding angle. Characteristic peaks of the FTO substrate is not valid peaks of the thin films studied. Characteristic peaks of the FTO substrate are neglected when the crystallite size is estimated from Scherrer formula. Similar crystallite size calculated using Scherrer formula can be found in [32]. Thus, the average crystallite size of pure Co_3O_4 (2θ=36.8°) calculated through above Scherrer formula is about 126 nm. As shown in curve b, the peaks are indexed to the composite of Co_3O_4 (JCPDS No. 73-1701) and RuO_2 (JCPDS No. 71-2273), together with characteristic peaks of the FTO substrate. The average crystallite size of 62.3% RuO_2 composite is about 34 nm according to Scherrer formula.

Morphology

Scanning electron microscope (SEM) images of 62.3% RuO_2 composite (a), 35.6% RuO_2 composite (b), 15.5% RuO_2 composite (c), and pure Co_3O_4 (d) are shown in Fig. 2. It can be clearly seen from Fig. 2a that the morphology of 62.3% RuO_2 composite consists of spherical-like particles with size of around 30 nm and highly porous structure. As the RuO_2 content decreases to 35.6%, the morphology changes with a slight size enlargement (30–40 nm) and porosity decreases (Fig. 2b). The size of particles (90–130 nm) sharply increases by decreasing RuO_2 content to 15.6% and porosity sharply decreases (Fig. 2c). The morphology of pure Co_3O_4 consists of elliptic-like particles with the largest particles size (100–250 nm) and the least porosity (Fig. 2d). The increase in particle size and decrease in porosity with the decrease of RuO_2 content can be explained as follows: Fine droplets of solution thermally decompose when a mixed solution of $RuCl_3$ and $Co(CH_3COO)_2{\cdot}4H_2O$ is sprayed on the hot FTO substrates. Thermal decomposition results in forming gases. Formation and amount of gases may have great influence

Fig. 2 SEM images of 62.3% RuO_2 composite (**a**), 35.6% RuO_2 composite (**b**), 15.5% RuO_2 composite (**c**), and pure Co_3O_4 (**d**)

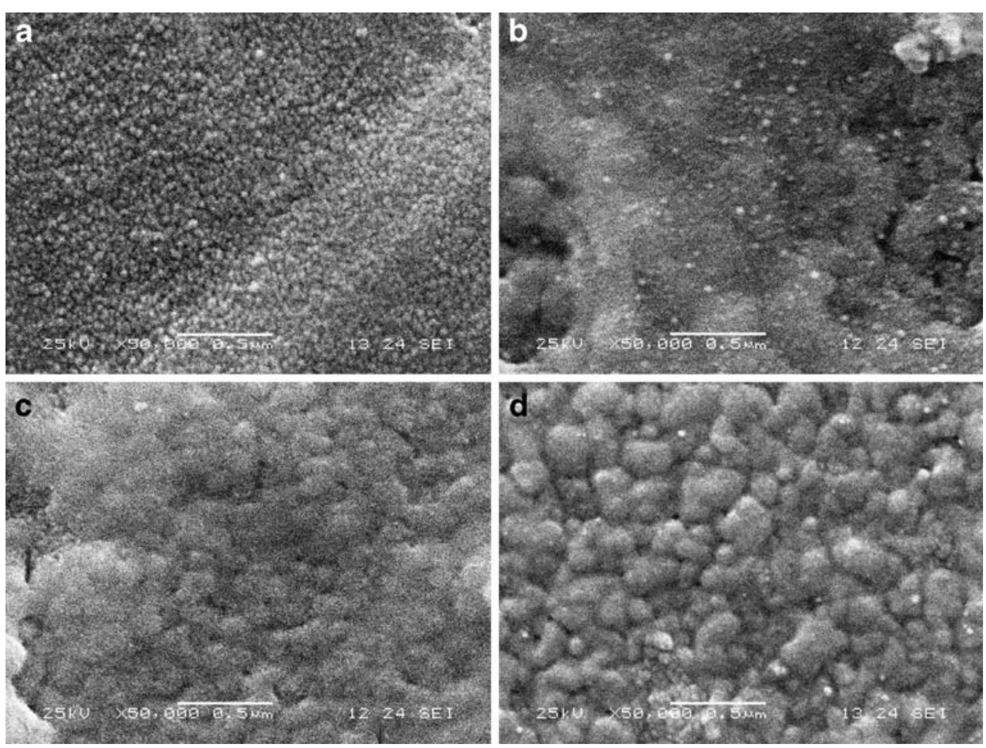

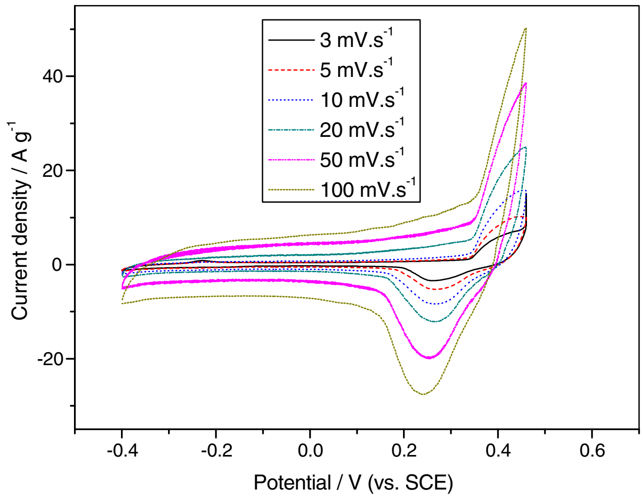

Fig. 3 Cyclic voltammograms of 62.3% RuO_2 composite film between −0.4 and 0.46 V in a 2-M KOH solution at different scan rates

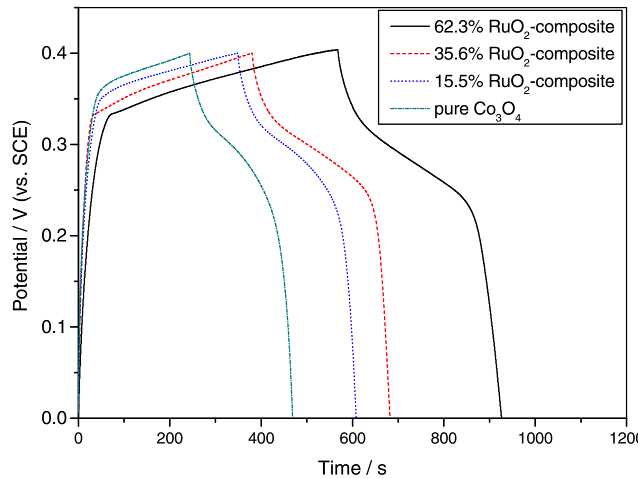

Fig. 5 The constant current charge/discharge curves of RuO_2/Co_3O_4 composite films with different RuO_2 content at the current density of 0.5 A g^{-1}

on the morphology of RuO_2/Co_3O_4 thin films. The particle size increases and porosity decreases with the decrease of RuO_2 content in RuO_2/Co_3O_4 thin films because of lower amount of gases during thermal decomposition of a mixed solution of $RuCl_3$ and $Co(CH_3COO)_2{\cdot}4H_2O$.

Electrochemical capacitor property

Figure 3 depicts cyclic voltammograms of 62.3% RuO_2 composite film between −0.4 and 0.46 V in a 2-M KOH solution at different scan rates ranging from 3 to 100 mV s^{-1}. The CV curves for Co_3O_4 and RuO_2 have been reported elsewhere [16, 30]. The shape of CV curves in Fig. 3 is considerably different from an ideal rectangular shape, indicating that capacitance mainly results from pseudocapacitance, which is caused by the fast and reversible faradaic redox reactions of electroactive material. The oxidation peak at about 0.45 V and the corresponding reduction peak at 0.268 V are observed in 2 M KOH solution at a scan rate of 10 mV s^{-1}. The voltage difference between the oxidation and reduction peak increases due to the polarization of electrode under high scan rate. Besides, the peak currents increased with the scan rate, which is interpreted based on rapid reversible redox reaction occurred among the electrode materials.

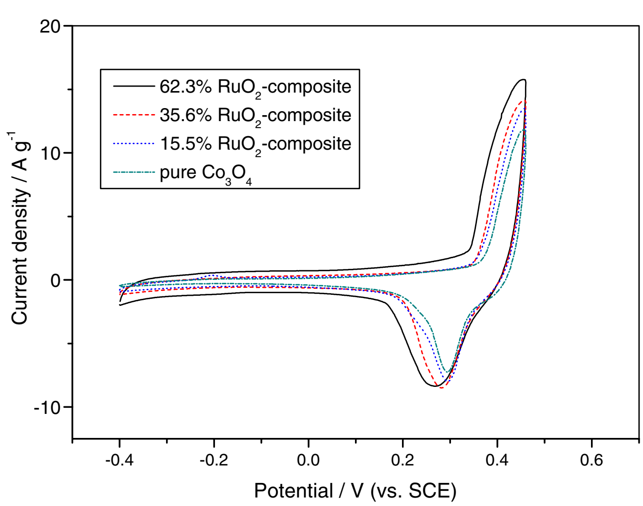

Fig. 4 Cyclic voltammograms of RuO_2/Co_3O_4 composite films with RuO_2 different content in a 2-M KOH solution at a scan rate of 10 mV s^{-1}

Figure 4 shows cyclic voltammograms RuO_2/Co_3O_4 composite films with different RuO_2 content in a 2-M KOH solution at a scan rate of 10 mV s^{-1}. The current increases with the increase of RuO_2 content, indicating 62.3% RuO_2 composite possesses the highest specific capacitance value. Besides, potential of reduction peak shift positively with the decrease of RuO_2 content. Potentials of reduction peak for 62.3% RuO_2, 35.6% RuO_2, 15.5% RuO_2, and pure Co_3O_4 are 0.268, 0.283, 0.293, and 0.295 V, respectively. The reason for the above phenomenon is different content of RuO_2 in RuO_2/Co_3O_4 composite films. In pure Co_3O_4, the oxidation peak is exhibited at about 0.45 V, and the corresponding reduction peak is 0.295 V. The redox peaks correspond to the electrode reaction as follows

$$CoOOH + OH^- \rightleftarrows CoO_2 + H_2O + e^- \quad (2)$$

This agrees with previous observations [16, 30, 33], where the CoOOH under open-circuit potential conditions is formed initially from

$$Co_3O_4 + H_2O + OH^- \rightleftarrows 3CoOOH + e^- \quad (3)$$

Table 1 The overall specific capacitance of composites (C_{sp}) and the corresponding contribution from RuO_2 (C_{sp}^{RuO2}) at various current densities

I/Ag^{-1}	62.3% RuO_2 composite		35.6% RuO_2 composite		15.5% RuO_2 composite		Pure Co_3O_4	
	C_{sp}/Fg^{-1}	C_{sp}^{RuO2}/F g^{-1}	C_{sp}/Fg^{-1}	C_{sp}^{RuO2}/Fg^{-1}	C_{sp}/Fg^{-1}	C_{sp}^{RuO2}/Fg^{-1}	C_{sp}/Fg^{-1}	C_{sp}^{RuO2}/Fg^{-1}
0.2	690±14	869±23	520±10	747±30	453±9	775±72	394±8	–
0.5	449±9	551±15	382±8	564±24	323±6	551±50	281±6	–
1.0	353±7	461±11	326±6	596±18	230±5	535±36	174±3	–
1.5	312±6	419±10	275±6	528±18	168±3	347±25	135±3	–
2.0	287±6	393±10	241±5	474±14	139±3	286±22	112±2	–

However, the following reaction exists in 15.5%, 35.6%, and 65.3% RuO_2 composite films except for above electrode reactions of Co_3O_4

$$RuO_2 + H_2O + e^- \rightleftarrows RuOOH + OH^- \quad (4)$$

Figure 5 displays the constant current charge/discharge curves of RuO_2/Co_3O_4 composite films with different RuO_2 content between 0 and 0.4 V in a 2-M KOH solution at the current density of 0.5 A g^{-1}. During charge and discharge, the curves are not linear, indicating that the capacitance performance is not pure electric double-layer capacitance, which is in agreement with CV curves in Fig. 4. There are two variation range of potential versus time during charge and discharge. A nonlinear variation of potential versus time is displayed, which may be a pseudocapacitance performance arisen from the electrochemical adsorption–desorption or redox reaction at an interface between the electrode and the electrolyte [34]. A linear variation of potential versus time is observed, which indicates electric double-layer capacitance rooted in the charge separation that took place between the electrode and the adjacent electrolyte interface.

The overall specific capacitance of RuO_2/Co_3O_4 composite films can be calculated by the following Eq. 5

$$C_{sp} = \frac{I \times t}{V \times m} \quad (5)$$

where I is the discharge current, t is the discharge time, V is the potential range during discharge, and m is the mass of RuO_2/Co_3O_4 composite films. The corresponding contribution from RuO_2 is calculated from RuO_2 content. The assumptions are as follows: (1) the total specific capacitance of composite films consists of RuO_2-specific capacitance and Co_3O_4-specific capacitance and (2) the Co_3O_4 specific capacitance is not affected by RuO_2 content. The overall specific capacitance of composites (C_{sp}) and the corresponding contribution from RuO_2 (C_{sp}^{RuO2}) at various current densities are listed in Table 1. The specific capacitance values of pure Co_3O_4, 15.5%, 35.6%, and 62.3% RuO_2 composites at the current density of 0.2 A g^{-1} are 394±8, 453±9, 520±10, and 690±14 F g^{-1}, respectively. These values are much higher than those of RuO_2/NiO materials prepared by Liu and Zhang (maximum value 210 F g^{-1}) [23] and RuO_2/SnO_2 materials prepared by Hu et

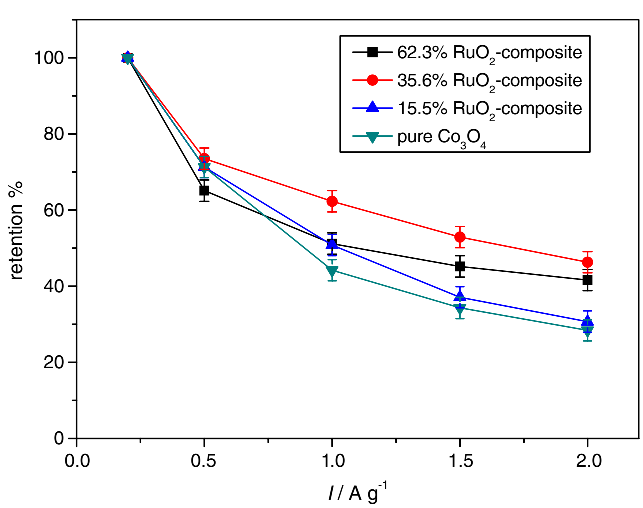

Fig. 6 The specific capacitance retention ratio as a function of the current density

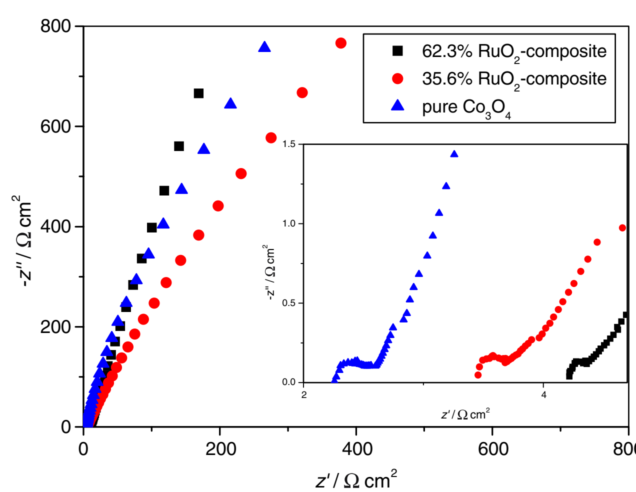

Fig. 7 The Nyquist impedance plots for 62.3% RuO_2 composite, 35.6% RuO_2 composite, and pure Co_3O_4 measured at bias potential of 0.3 V

al. (136–362 F g^{-1}) [25]. Table 1 also clearly shows that the reduction in RuO_2 content reduces drastically the overall specific capacitance. In other words, 62.3% RuO_2 composite presented the highest specific capacitance value at various current densities. This is because RuO_2 possesses higher energy storage capabilities with larger specific capacitance than other transition metal oxides. The C_{sp}^{RuO2} of 62.3%, 35.6%, and 15.5% RuO_2 composites at the current density of 0.2 A g^{-1} in Table 1 are 869±23, 747±30, and 775±72 F g^{-1}, respectively, which are comparable with that of amorphous ruthenium oxide (720 F g^{-1}) [35]; 35.6% RuO_2 composite exhibits the largest C_{sp}^{RuO2} which are 564±24, 596±18, 528±18, and 474±14 F g^{-1} at the current density of 0.5, 1.0, 1.5, and 2.0 A g^{-1}, respectively. The main reason for the above behavior may be attributed to be fully utilized for charge storage in 35.6% RuO_2 composite, which is based on different microstructure and surface morphology of the RuO_2/Co_3O_4 composites. On the other hand, the decrease in overall specific capacitance with current density is more significant for low load of RuO_2. The specific capacitance retention ratio as a function of the current density is shown in Fig. 6. The highest ratio (46.3±2.8%) is obtained in 35.6% RuO_2 composite at the current density ranging from 0.2 to 2.0 A g^{-1}. These results indicate that 35.6% RuO_2 composite suits to high-rate charge–discharge. The above results can be explained as follows: A lower electron hopping resistance results in a lower iR at a high-rate charge–discharge for 35.6% RuO_2 composite.

Figure 7 presents the Nyquist impedance plots for 62.3% RuO_2 composite, 35.6% RuO_2 composite, and pure Co_3O_4 measured at bias potential of 0.3 V versus SCE in a 2-M KOH solution in the frequency range 0.01~10^5Hz. In the high frequency range, the intercept at real part (Z') is a combinational resistance of ionic resistance of electrolyte, intrinsic resistance of substrate, and contact resistance between the active material and the current collector [36]. These values for 62.3% RuO_2 composite, 35.6% RuO_2 composite, and pure Co_3O_4 are 4.23, 3.46, and 2.23 Ω cm^2, respectively. Since resistance of ionic resistance of electrolyte and intrinsic resistance of substrate are the same for all the samples, the different values imply the difference of the contact resistance between the active material and the current collector. The contact resistance of different RuO_2/Co_3O_4 composites drops gradually with the decrease of RuO_2 content. The depressed semicircle is observed in the high frequency region, which results from a parallel combination of the charge-transfer resistance (R_{ct}) caused by faradaic reactions and the double-layer capacitance (C_{dl}) [36]. The charge-transfer resistance (R_{ct}) from the diameter of the semicircle for 62.3% RuO_2 composite, 35.6% RuO_2 composite, and pure Co_3O_4 is estimated ca. 0.17, 0.24, and 0.32 Ω cm^2, respectively. The charge-transfer resistance (R_{ct}) increases gradually with the decrease of RuO_2 content. In the low frequency range, impedance plots show nearly vertical lines, which is an ideal capacitive behavior.

Conclusions

RuO_2/Co_3O_4 composites with various RuO_2 content have been prepared on FTO substrates by spray pyrolysis method, and their capacitive behavior has been investigated. Based on CV and constant current charge/discharge results, capacitance of RuO_2/Co_3O_4 composites with various RuO_2 content mainly results from pseudocapacitance. The specific capacitance of pure Co_3O_4, 15.5%, 35.6%, and 62.3% RuO_2 composites at the current density of 0.2 A g^{-1} are 394±8, 453±9, 520±10, and 690±14 F g^{-1}, respectively; 62.3% RuO_2 composite possesses the highest specific capacitance value at various current densities, and 35.6% RuO_2 composite exhibits not only the largest specific capacitance contribution from RuO_2 (C_{sp}^{RuO2}) at the current density of 0.5, 1.0, 1.5, and 2.0 A g^{-1} but also the highest specific capacitance retention ratio (46.3±2.8%) at the current density ranging from 0.2 to 2.0 A g^{-1}. In conclusion, 35.6% RuO_2 composite is a economic material and suits to high-rate charge–discharge. Electrochemical impedance spectra show that the contact resistance drops gradually with the decrease of RuO_2 content, and the charge-transfer resistance (R_{ct}) increases gradually with the decrease of RuO_2 content. Further, this study provides a simple and economic available method to prepare RuO_2 loading in other transition metal oxides.

Acknowledgments Support of this work by grants from the National Natural Science Foundation of China (No. 20376085, No. E50772133) and Scientific Research Fund of Hunan Provincial Education Department (No. 09C1055) is gratefully appreciated.

References

1. Centeno TA, Stoeckli F (2006) Electrochim Acta 52:560
2. Qu D (2002) J Power Sources 109:403
3. Hu CC, Chang KH, Lin MC, Wu YT (2006) Nano Lett 6:2690
4. Liang Y-Y, Li HL, Zhang X-G (2007) J Power Sources 173:599
5. Fang W-C, Huang J-H, Chen L-C, Su Y-LO, Chen K-H (2006) J Power Sources 160:1506
6. Hu C-C, Chen W-C, Chang K-H (2004) J Electrochem Soc 151:A281
7. Brousse T, Toupin M, Dugas R, Athouel L, Crosnier O, Belanger D (2006) J Electrochem Soc 153:A2171
8. Nagarajan N, Humadi H, Zhitomirsky I (2006) Electrochim Acta 51:3039
9. Nakayama M, Kanaya T, Inoue R (2007) Electrochem Commun 9:1154
10. Huang Q, Wang X, Li J (2006) Electrochim Acta 52:1758
11. Cheng J, Cao G-P, Yang Y-S (2006) J Power Sources 159:734
12. Lee S-H, Tracy CE, Pitts JR (2004) Electrochem Solid St 7:A299
13. Wu M-S, Huang Y-A, Yang C-H, Jow J-J (2007) Int J Hydrogen Energy 32:4153

14. Kim H-K, Seong T-Y, Lim J-H, Ii Cho W, Soo Yoon Y (2001) J Power Sources 102:167
15. Shinde VR, Mahadik SB, Gujar TP, Lokhande CD (2006) Appl Surf Sci 252:7487
16. Chuan L, James AR, Branko NP (1998) J Electrochem Soc 145:4097
17. Liu TC, Pell WG, Conway BE (1999) Electrochim Acta 44:2829
18. Yuan C, Zhang X, Gao B, Li J (2007) Mater Chem Phys 101:148
19. Yu W, Yang X, Wang P, Meng L (2006) ECS Transactions 1:19
20. Mastragostino M, Arbizzani C, Soavi F (2002) Solid State Ionics 148:493
21. Soudan P, Ho HA, Breau L, Belanger D (2001) J Electrochem Soc 148:A775
22. Wu M, Zhang L, Wang D, Xiao C, Zhang S (2008) J Power Sources 175:669
23. Liu XM, Zhang XG (2004) Electrochim Acta 49:229
24. Pico F, Ibanez J, Centeno TA, Pecharroman C, Rojas RM, Amarilla JM, Rojo JM (2006) Electrochim Acta 51:4693
25. Hu C-C, Chang K-H, Wang C-C (2007) Electrochim Acta 52:4411
26. Wang Y-G, Wang Z-D, Xia Y-Y (2005) Electrochim Acta 50:5641
27. Ye J-S, Cui HF, Liu X, Lim TM, Zhang W-D, Sheu F-S (2005) Small 1:560
28. Jang JH, Han S, Hyeon T, Oh SM (2003) J Power Sources 123:79
29. Liu Y, Zhao W, Zhang X (2008) Electrochim Acta 53:3296
30. Krstajic N, Trasatti S (1995) J Electrochem Soc 142:2675
31. Gujar TP, Shinde VR, Lokhande CD, Kim W-Y, Jung K-D, Joo O-S (2007) Electrochem Commun 9:504
32. Desai JD, Min S-K, Jung K-D, Joo O-S (2006) Appl Surf Sci 253:1781
33. Švegl F, Orel B, Hutchins MG, Kalcher K (1996) J Electrochem Soc 143:1532
34. Tao F, Zhao Y-Q, Zhang G-Q, Li H-L (2007) Electrochem Commun 9:1282
35. Zheng JP, Cygan PJ, Jow TR (1995) J Electrochem Soc 142:2699
36. Wu M-S, Hsieh H-H (2008) Electrochim Acta 53:3427